

Tables DR1-DR3: 2018177 TablesDR1-DR3.xls

File DR1 – SAMPLE DESCRIPTIONS

Sample ID	Location		Notes (mineralogy, major phases)
	Latitude/ Longitude	Project	
KA15_004	41.005° N 25.749° E	Kassiteres	Diorite – plagioclase + clinopyroxene + hornblende + magnetite
KA15_008	40.999° N 25.740° E	Kassiteres	Diorite – plagioclase + hornblende + clinopyroxene + K-feldspar + quartz + magnetite
KA15_009	40.994° N 25.733° E	Kassiteres	Granodiorite – plagioclase + hornblende + K-feldspar + quartz + magnetite
KA15_013	40.996° N 25.748° E	Kassiteres	Granodiorite – plagioclase + hornblende + K-feldspar + quartz + magnetite
KA15_016	40.992° N 25.731° E	Kassiteres	Granodiorite – plagioclase + hornblende + K-feldspar + quartz + magnetite
KA15_017	40.996° N 25.735° E	Kassiteres	Granodiorite – plagioclase + hornblende + K-feldspar + quartz + magnetite
RT14_028 ^{1,2}	41.005° N 25.746° E	Kassiteres	Diorite – plagioclase + hornblende + clinopyroxene + K-feldspar + quartz + magnetite
RT14_026 ²	41.021° N 25.761° E	Kassiteres	Granodiorite – plagioclase + K-feldspar + hornblende + quartz + magnetite with intense chloritisation
RT14_022 ^{1,2}	41.035° N 25.819° E	Leptokaria	Granodiorite with propylitic alteration – plagioclase + clinopyroxene + amphibole + quartz + K-feldspar + magnetite
RT14_024 ^{1,2}	41.027° N 25.791° E	Leptokaria	Diorite with propylitic alteration – plagioclase + clinopyroxene + chlorite + biotite + magnetite
RT14_025 ³	41.027° N 25.791° E	Leptokaria	Gabbro – intensely propylitically altered (chlorite + epidote) – relict clinopyroxene + plagioclase + magnetite
LA15_009	41.066° N 25.904° E	Leptokaria	Granodiorite – plagioclase + hornblende + clinopyroxene + quartz + magnetite
LA15_011	41.077° N 25.924° E	Leptokaria	Granite – K-feldspar + plagioclase + quartz + hornblende + biotite + clinopyroxene + magnetite
RT14_009 ^{1,2}	41.060° N 25.911° E	Leptokaria	Granite – k-feldspar + plagioclase + quartz + hornblende + biotite + clinopyroxene + magnetite
LB15_003	41.092° N 25.961° E	Leptokaria	Tonalite – Plagioclase + quartz + hornblende + magnetite
LB15_004	41.086° N 25.972° E	Leptokaria	Granite with epidote veining – K-feldspar + quartz + plagioclase + hornblende + biotite + magnetite
LB15_006	41.085° N 25.972° E	Leptokaria	Granite with epidote veining – K-feldspar + plagioclase + quartz + hornblende + magnetite
RT14_017 ²	41.091° N 25.966° E	Leptokaria	Quartz-monzonite cumulate with epidote veining – hornblende + plagioclase + quartz + K-feldspar + magnetite
LC15_002	41.117° N 26.004° E	Leptokaria	Tonalite porphyry – plagioclase + hornblende + quartz phenocrysts
LC15_003	41.117° N 26.004° E	Leptokaria	Diorite – plagioclase + hornblende + clinopyroxene + biotite + quartz + magnetite

RT14_010 ^{1,2}	41.117° N 26.001° E	Leptokaria	Tonalite with minor chlorite alteration – plagioclase + quartz + K-feldspar + hornblende + chlorite + magnetite
LD15_002	41.146° N 26.049° E	Leptokaria	Gabbro – clinopyroxene + orthopyroxene + hornblende + plagioclase + magnetite
LD15_003	41.146° N 26.049° E	Leptokaria	Quartz monzonite with epidote veining – K-feldspar + plagioclase + clinopyroxene + quartz + magnetite
RT15_015 ²	41.141° N 26.042° E	Leptokaria	Diorite with minor chlorite alteration – plagioclase + biotite + hornblende + magnetite
MA15_004	40.866° N 25.549° E	Maronia	Monzonite – plagioclase + clinopyroxene + orthopyroxene + biotite + K-feldspar + magnetite + quartz + secondary amphibole
MA15_006	40.869° N 25.552° E	Maronia	Monzonite – plagioclase + clinopyroxene + orthopyroxene + biotite + K-feldspar + magnetite + quartz + secondary amphibole
MA15_007	40.869° N 25.552° E	Maronia	Monzonite – plagioclase + clinopyroxene + orthopyroxene + biotite + K-feldspar + magnetite + quartz + secondary amphibole
MA15_008	40.869° N 25.551° E	Maronia	Monzonite – plagioclase + clinopyroxene + orthopyroxene + biotite + K-feldspar + magnetite + quartz + secondary amphibole
MA15_010 ¹	40.861° N 25.565° E	Maronia	Monzonite – plagioclase + clinopyroxene + orthopyroxene + biotite + K-feldspar + magnetite + quartz + secondary amphibole
MA15_011	40.860° N 25.565° E	Maronia	Monzonite – plagioclase + clinopyroxene + orthopyroxene + biotite + K-feldspar + magnetite + quartz + secondary amphibole
MA15_012	40.862° N 25.564° E	Maronia	Monzonite – plagioclase + clinopyroxene + orthopyroxene + biotite + K-feldspar + magnetite + quartz + secondary amphibole
MA15_014	40.873° N 25.540° E	Maronia	Monzonite – plagioclase + clinopyroxene + orthopyroxene + biotite + K-feldspar + magnetite + quartz + secondary amphibole
MA15_015	40.873° N 25.538° E	Maronia	Monzonite – plagioclase + clinopyroxene + orthopyroxene + biotite + K-feldspar + magnetite + quartz + secondary amphibole
MA15_016	40.872° N 25.536° E	Maronia	Monzonite – plagioclase + clinopyroxene + orthopyroxene + biotite + K-feldspar + magnetite + quartz + secondary amphibole
MA15_017	40.865° N 25.538° E	Maronia	Monzonite – plagioclase + clinopyroxene + orthopyroxene + biotite + K-feldspar + magnetite + quartz + secondary amphibole
MA15_020	40.877° N 25.538° E	Maronia	Monzonite – plagioclase + clinopyroxene + orthopyroxene + biotite + K-feldspar + magnetite + quartz + secondary amphibole
RT14_003 ^{1,2}	40.862° N 25.565° E	Maronia	Monzonite – plagioclase + clinopyroxene + orthopyroxene + biotite + K-feldspar + magnetite + quartz + secondary amphibole
RT14_006 ²	40.867° N 25.539° E	Maronia	Monzonite – plagioclase + clinopyroxene + orthopyroxene + biotite + K-feldspar + magnetite + quartz + secondary amphibole
MN16_008 ^{1,3}	40.879° N 25.547° E	Maronia	Monzonite – plagioclase + clinopyroxene + orthopyroxene + biotite + K-feldspar + magnetite + quartz + secondary amphibole
MN16_005 ^{1,3}	40.879° N 25.554° E	Maronia	Monzonite – plagioclase + clinopyroxene + orthopyroxene + biotite + K-feldspar + magnetite + quartz + secondary amphibole

Table 1: Locations (WGS84) and descriptions of each of the samples used in this study. ¹ denotes samples used for geochronology, ² samples with thin sections selected for point counting and ³ samples that do not have a whole rock analysis.

FILE DR2 – U-PB ZIRCON GEOCHRONOLOGY

This section of the supplementary material covers a detailed outline of sample selection, analytical procedure and data interpretation of the CA-ID-TIMS (Chemical Abrasion Isotope Dilution Thermal Ionisation Mass Spectrometry) U-Pb in zircon geochronology.

2 1 – Dating Methods

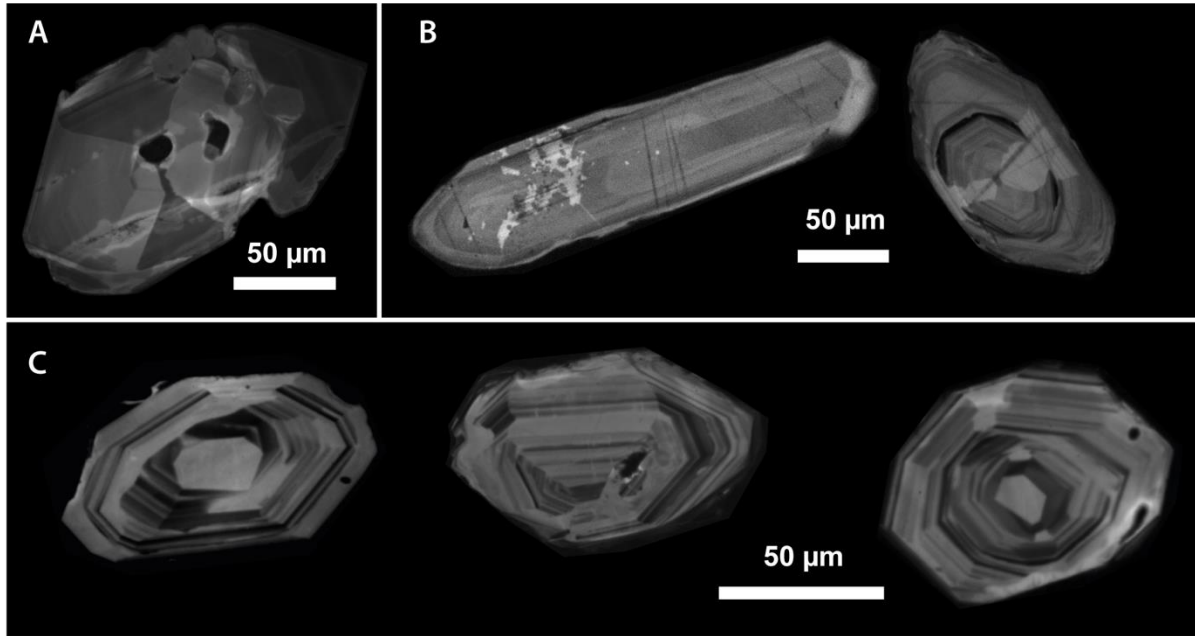


Figure 1: Representative cathodoluminescence images of zircons from the MMC. Zircons range in size from 250 to 75 μm , are typically euhedral and show simple oscillatory and sector zoning with little evidence of magmatic resorption or inheritance in all samples. A) Maronia: Zircons have abundant inclusions of apatite or melt. B) Kassiteres: Zircons commonly show evidence of hydrothermal fluid activity e.g. the mottled white texture in the left zircon. C) Leptokaria: Zircons are typically very simple.

2.1.1 – Cathodoluminescence Imagery and Crystal Selection

A total of nine samples were collected from the Maronia Magmatic Corridor (MMC) for geochronology in this study, five from the Kassiteres – Leptokaria magmatic suite and four from the Maronia plutonic complex. Over 3 kg of rock was collected for each sample to provide sufficient material for zircon mineral separation. Samples were crushed, sieved, rinsed and density separated following standard procedures at the University of Bristol. Individual zircon crystals were picked from the 50 – 250 μm size fraction (20 – 50 for each sample).

After crystal selection, the remaining zircons were mounted in epoxy resin and polished for scanning electron microscope (SEM) work. Cathodoluminescence (CL) imaging revealed simple zoning patterns in most all of the zircons from the MMC pluton samples (Figure 1). Oscillatory and sector zoning in the zircon crystals reflect a single zircon crystallisation event in each of the plutons with no evidence of zircon resorption or inheritance reflecting multiple period of crystallisation.

2.1.2 – Chemistry, Mass Spectrometry and Corrections

Zircons selected for analysis were chemically abraded following a modified procedure from Mattinson, (2005) to remove damaged parts of the crystal that were likely to have experienced open-system behaviour. Firstly, the zircons were thermally annealed at 900 $^{\circ}\text{C}$ for 60 hours in quartz crucibles before

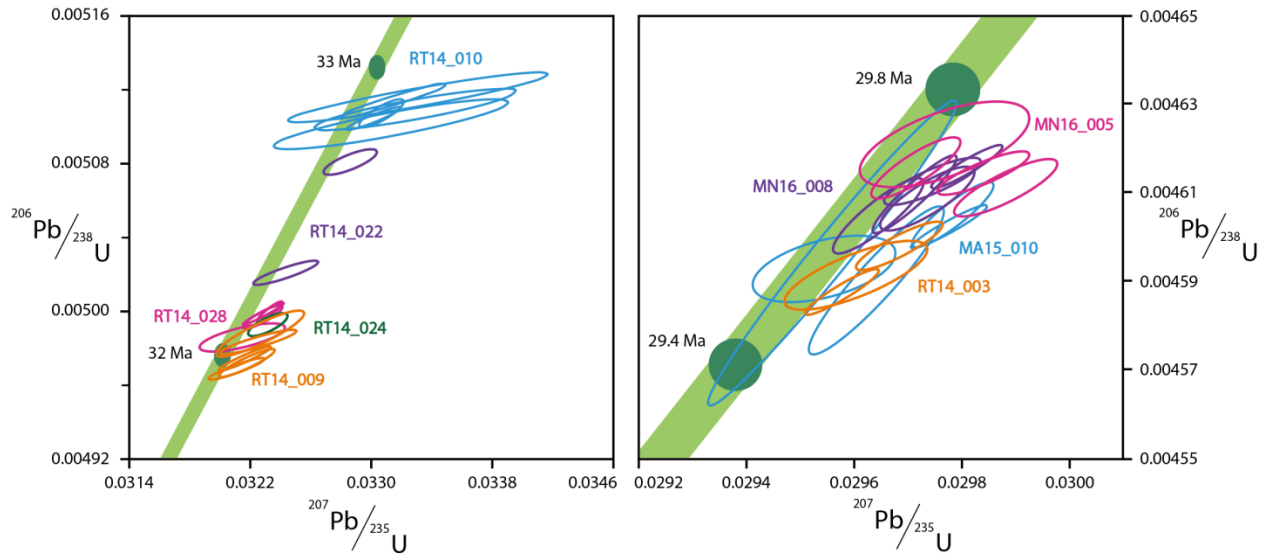
being individually selected, photographed and loaded into FEP Teflon beakers. Single zircon crystals, or fragments, were selected for dissolution using transmitted light microscopy. Zircons were selected based upon their external morphology and observation of internal feature (i.e., visible cores).

Zircons were then refluxed in 4 M HNO₃ on a hotplate at 120 °C for > 2 hours, followed by ultrasonic cleaning for at least 20 minutes. The zircon crystals were rinsed with acetone and 4 M HNO₃ and loaded into individual 300 µl FEP Teflon microcapsules and leached in 29 M HF inside a Parr vessel (a self-sealing stainless-steel jacket) for 12 hours at 180 °C. The zircons were rinsed with 4 M HNO₃ and refluxed in 6 M HCl at 120 °C for 2-5 hours, before a final rinsing with 4 M HNO₃ several times.

The leached zircons and all total procedural blanks were spiked with mixed ²⁰⁵Pb – ²³³U – ²³⁵U (ET535) EARTHTIME tracer solution and dissolved in ~150 µl 29 M HF and trace HNO₃ in a Parr vessel at 220 °C for at least 60 hours. Complete dissolution was checked by visual inspection of some larger crystals and assumed for smaller grains, following standard protocol for dissolution at NIGL. The solutions were dried down as fluorides and re-dissolved in 3 M HCl in a Parr vessel overnight at 180 °C. U and Pb fractions were isolated by a HCl-based anion exchange procedure using Bio-Rad AG-1 resin in Teflon columns. Pb and U fractions were then recombined and dried down with ~10 µl of H₃PO₄. The dried samples were then loaded onto zone-refined Re filaments in a silica gel matrix to enhance ionisation (after Gerstenberger & Haase, 1997).

Isotope ratios were measured on a Thermo-Electron Triton thermal ionisation mass spectrometer (TIMS). Pb was measured in dynamic mode on a MassCom secondary electron multiplier; Pb mass bias corrections were made using a fractionation factor of $0.14 \pm 0.02 \text{ \% amu}^{-1}$ (1 sigma) for samples spiked using ET535. Dead-time and linearity of the secondary electron multiplier were monitored using repeated analyses of the standards NBS 982, NBS 981 and U 500. U oxide (UO₂) was measured, and corrected for isobaric interferences using a ¹⁸O/¹⁶O value of 0.00205 (IUPAC value and measured in-house at NIGL). U was measured in dynamic mode and a mass bias fractionation correction calculated in real-time using the ²³³U-²³⁵U ratio of the ET535 tracer solutions (Condon et al., 2015). Corrections for the addition of Pb and U during the procedure (i.e., laboratory contamination) were made using the long-term measured isotopic composition and variability of blanks using an amount that is based upon contemporary total procedural blanks. The U/Pb ratio for each analyses was determined via isotope dilution principles and the ET535 mixed ²⁰⁵Pb-²³³U-²³⁵U tracer (Condon et al., 2015; McLean et al., 2015). A ²³⁸U/²³⁵U value of 137.818 (Hiess et al., 2012) was assumed and used in the data reduction algorithm.

Figure 2: Concordia plot of the Kassiteres - Leptokaria samples (left) and the Maronia samples (right). Note the horizontal translation of the data points off Concordia with excess ^{207}Pb .



SB 1.3 – U-Pb Data, Corrections and Assessment

Once the radiogenic isotopic compositions ($^{206}\text{Pb}/^{238}\text{U}$ and $^{207}\text{Pb}/^{235}\text{U}$) have been determined for a given analyses/zircon a number of factors must be considered prior to geochronological interpretation (i.e., age assignment).

Initial ^{230}Th disequilibrium. Due to the slightly larger ionic radius of Th the intermediate daughter ^{230}Th is excluded during zircon crystallisation such that a correction is required to account for ^{230}Th disequilibrium and resulting in deficit ^{206}Pb (e.g. Schärer 1984; Parrish 1990). This disequilibrium correction requires a priori knowledge of the Th/U of the magma coexisting with the crystal during

growth. A sensitivity analysis of the choice of Th/U ratio in the Th-correction shows an inverse exponential relationship between the magnitude of the Th-correction and Th/U ratio that plateaus between Th/U = 3-4 (Figure 1). It is not possible to account for the excess ^{207}Pb by the Th-correction alone. The whole rock Th/U ratio of the full MMC suite varies between 3 and 5.5. A value of Th/U = 3.5 was selected for the Th-correction in this study.

Concordance of U-Pb system. Once this correction has been applied it is noticeable that in general the U-Pb are discordant with $^{207}\text{Pb}/^{235}\text{U}$ dates $>$ $^{206}\text{Pb}/^{238}\text{U}$ dates (Figure 1). The U-Pb analyses from the MMC plot off Concordia in some, if not all analyses, from 8 out of 9 samples. The discordance could reflect either excess ^{207}Pb and/or lost ^{235}U or inheritance. In the case of inheritance of an older zircon core, the data would plot on a chord intersecting Concordia an older age (e.g. the xenocrystic zircons from RT14_024). However, the deviation from Concordia of most all data is a horizontal translation of the analyses interpreted as autocrystic youngest zircons. We consider what could be causing this.

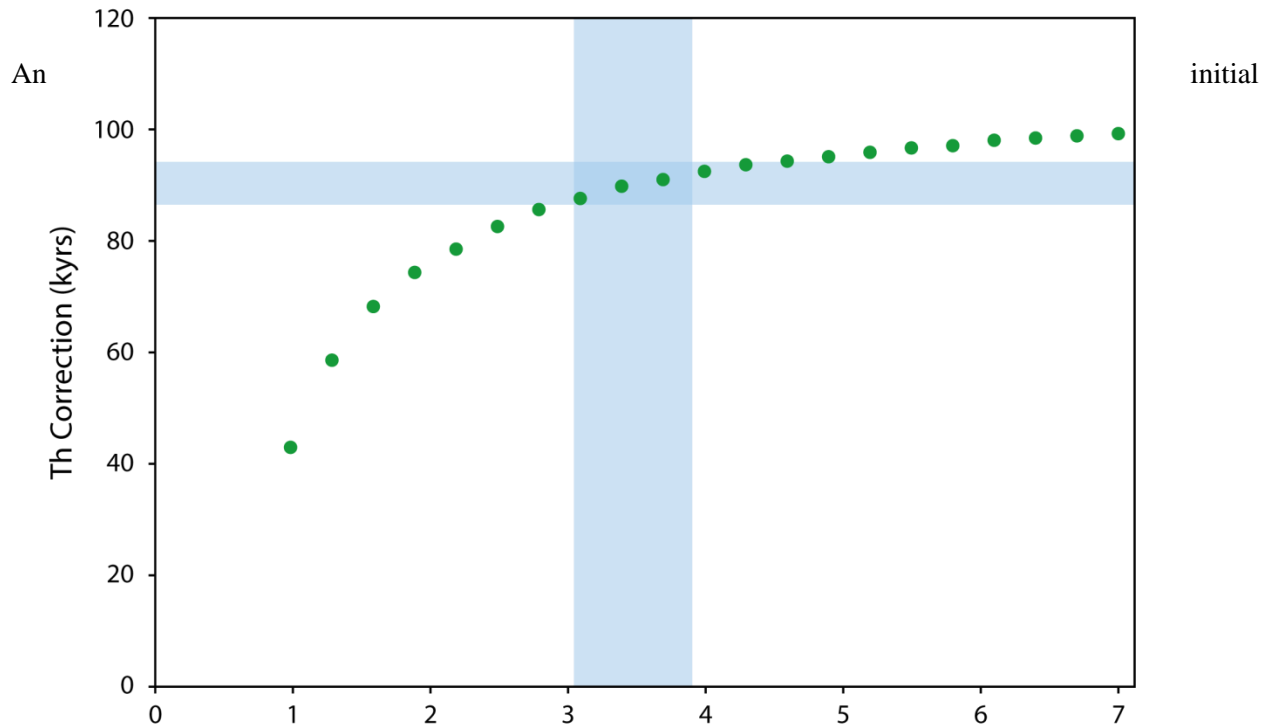
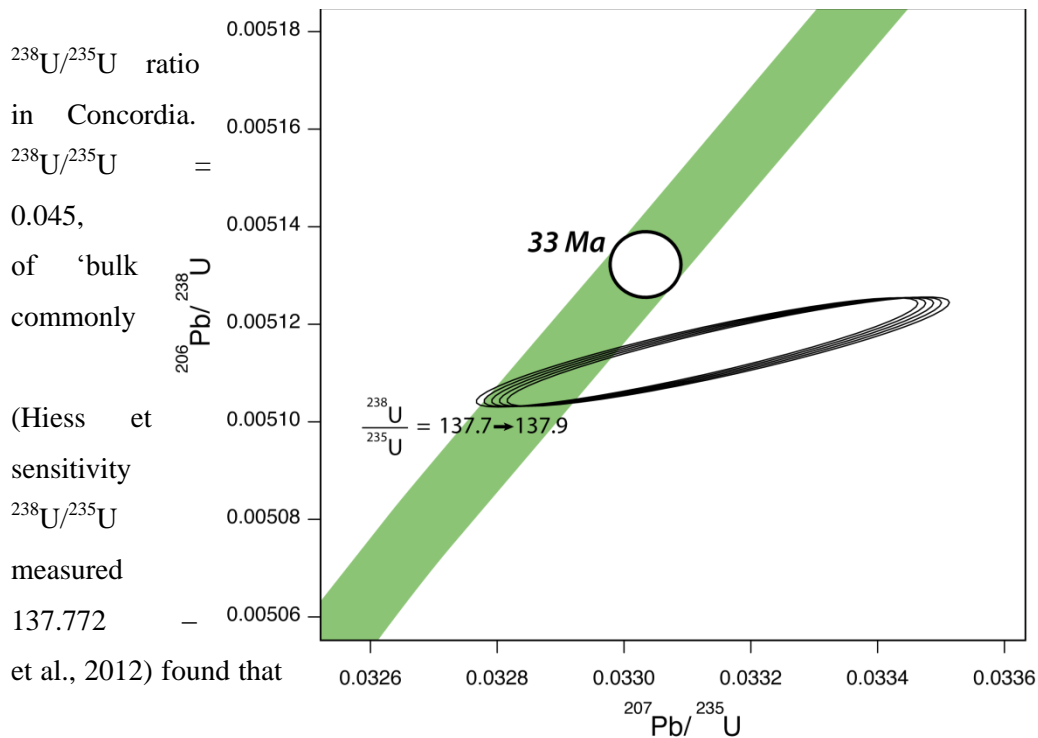


Figure 3 (above): A sensitivity test of the magnitude of the Th-correction with varying Th/U ratio. In order to match the discordance observed in the data a large Th-correction is needed to account for excess ^{207}Pb compared to ^{206}Pb . There is an inverse exponential relationship between Th/U ratio and the magnitude of the Th-correction which plateaus at a Th-correction of 90 kyrs when Th/U > 3. Therefore, the discordance in the data (> 100,000 kyrs for each sample) cannot be accounted for solely by changing the Th/U ratio.

Figure 4 (below): Sensitivity test of the $^{238}\text{U}/^{235}\text{U}$ ratio and the concordance of the $^{207}\text{Pb}/^{235}\text{U}$ and $^{206}\text{Pb}/^{238}\text{U}$ ages, a concordant analysis would lie on the green Concordia line (with decay constant uncertainty). Increasing the $^{238}\text{U}/^{235}\text{U}$ ratio used can horizontally shift the data points away from Concordia affecting only the $^{207}\text{Pb}/^{235}\text{U}$ age. However, the magnitude of this shift is small and cannot account for the discordance seen in our dataset.



$^{238}\text{U}/^{235}\text{U}$ ratio
in Concordia.
 $^{238}\text{U}/^{235}\text{U} = 0.045$,
of 'bulk
commonly
(Hiess et
sensitivity
 $^{238}\text{U}/^{235}\text{U}$
measured
137.772

et al., 2012) found that

is also assumed
A value of
137.818 ±
representative
Earth', is
used in U-Pb
calculations
al., 2012). A
analysis of the
within the
terrestrial range
137.908 (Hiess
the initial

assumed $^{238}\text{U}/^{235}\text{U}$ cannot account for excess ^{207}Pb observed in the discordant data (Figure 2). The ‘bulk Earth’ value of $^{238}\text{U}/^{235}\text{U} = 137.818 \pm 0.045$ has been used in this study.

We do not consider that the laboratory procedure introduced a systematic or random bias into the analyses as the data were collected in numerous sessions of column chemistry and mass spectrometer analysis over a number of years at NIGL. The high Pb^*/Pb_c ratios indicate this is not a likely cause of the discordance, and a sensitivity analyses confirms this (i.e., a non-terrestrial Pb_c composition would be required). Furthermore, such discordance is not observed in other similar age zircons made following the same laboratory protocol conducted at NIGL and with lower Pb^*/Pb_c (Sahy et al., 2015).

Previous work has encountered similar ^{207}Pb excess which cannot be accounted for by assumptions in the data reduction or by laboratory procedure (e.g. Crowley et al., 2007). The discordance has been attributed to initial Pa/U disequilibrium from the partitioning of excess Pa into the zircon, which is significant only in very reduced or young (Cenozoic) systems (e.g. Schmitt 2007). Crowley et al., (2007) attribute the 52,000 yr bias between their $^{206}\text{Pb}/^{238}\text{U}$ and $^{207}\text{Pb}/^{235}\text{U}$ dates of the Bishop Tuff to Pa/U disequilibrium and suggest that similar variations could be observed in rocks < 10 Ma. We suggest that Pa/U disequilibrium is accountable for the average 23,000 yr difference between $^{206}\text{Pb}/^{238}\text{U}$ and $^{207}\text{Pb}/^{235}\text{U}$ dates. To conclude, we believe that this discordance between the $^{207}\text{Pb}/^{235}\text{U}$ and $^{206}\text{Pb}/^{238}\text{U}$ is real and proceed to interpret the (^{230}Th corrected) $^{206}\text{Pb}/^{238}\text{U}$ dates as being geologically meaningful as they are unaffected by the ^{207}Pb from Pa disequilibrium.

2.2 – Zircon U-Pb Data Interpretation

Date – the calculated time since closure of a system in a single analysis.

Age – the geological interpretation of a collection of dates from a single sample and represents the final interpretation of the timing of a geological event.

U-Pb in zircon is a long-lived radiogenic isotopic geochronometer that is used across geological disciplines to constrain the timing of geological events. In plutonic systems, the U-Pb system is used to date crystallisation of zircon from the magma as the closure temperature of the isotopic systems is ~ 900 °C, well above the zircon saturation temperature of most evolved magmatic systems. In order to constrain the final stages of pluton crystallisation, the time of emplacement, the youngest zircon from the system would ideally be dated. In the absence of dating all of the zircons from a single plutonic system to

constrain emplacement, the youngest analysis or cluster of analyses (i.e. $^{206}\text{Pb}/^{238}\text{U}$ dates), is frequently interpreted as the crystallisation age of the magmatic system. Older dates from the same sample are interpreted as antecrystic, reflecting the lifespan of the magmatic system with crystallisation occurring over a period of 10,000s to 100,000s yrs prior to final emplacement (e.g. von Quadt et al., 2011). If the youngest, single, zircon date is used to interpret the pluton emplacement with a 95 % confidence level then in 1 out of 20 scenarios the actual age of zircon will fall outside of the given value. In order to combat this, populations of zircons are used and rely on the reproducibility of analyses to reduce the uncertainty associated with data interpretation.

Below we outline the multiple interpretations of the analyses of each sample from this study and show that to the degree the data is interpreted in this study, the choice of interpretation makes little difference for most samples. In general, our approach is to derive a sample age based upon a weighted mean (Th-corrected) $^{206}\text{Pb}/^{238}\text{U}$ date derived from the youngest coherent population. This allows for ages to be based upon reproduced $^{206}\text{Pb}/^{238}\text{U}$ and not a single analysis. The coherence of a dataset was decided based upon the MSWD (mean square weighted deviation – a chi –squared statistical test; Wendt & Carl 1991) where values exceeding that expected for the given sample size indicate excess scatter and the likely presence of pre-eruptive zircon.

2.2.1 – The Kassiteres – Leptokaria Magmatic Suite

Five samples were selected for U-Pb geochronology from the Kassiteres – Leptokaria Magmatic Suite to represent intra-system variability in crystallisation ages and estimate the lifespan of magmatic system. Autocrystic zircon analyses, those interpreted to reflect the final stages of crystallisation, range in age from 32.03 to 32.98 Ma suggested pulsed magma accumulation and crystallisation in the Kassiteres – Leptokaria system over a period of at least 1 Myrs.

Analyses of RT14_009 range between 32.10 and 32.30 Ma ($^{206}\text{Pb}/^{238}\text{U}$ dates, $n = 7$). There are three interpretations of these analyses: 1) the samples represent a single population with an interpreted geological age of 32.225 ± 0.036 (MSWD = 5.2, $n = 7$), however, the MSWD is too high (if $n = 7$, $\text{MSWD} < 2.26$ at 2σ confidence levels) to represent a statistically significant population indicating over-dispersion of the data; 2) the youngest analysis represents a maximum age of final crystallisation of the intrusion of 32.14 ± 0.04 Ma; 3) as all the analyses overlap within error, our favoured approach is to exclude the outlying youngest analysis and interpret a geological age of 32.235 ± 0.026 Ma (MSWD = 2.2, $n = 6$).

Analyses of RT14_010 range between 32.82 and 33.05 Ma ($^{206}\text{Pb}/^{238}\text{U}$ dates, $n = 6$). Our favoured interpretation of these analyses is that the data represent a single population of zircons with an interpreted $^{206}\text{Pb}/^{238}\text{U}$ geological age of 32.932 ± 0.034 Ma (MSWD = 2.9, $n = 6$); the MSWD is fractionally too high indicating mild over-dispersion of the data (if $n = 6$, MSWD < 2.41 at 2σ confidence levels). An alternative approach would be to reject the older two analyses as an antecrystic zircons and interpret a youngest population with a geological age of 32.917 ± 0.021 Ma (MSWD = 0.87, $n = 4$).

Analyses of RT14_022 range between 36.05 and 32.35 Ma ($^{206}\text{Pb}/^{238}\text{U}$ dates, $n = 3$). The anomalously old date calculated for one of these zircon analyses (35.94 ± 0.11 Ma) suggests an xenocrystic origin of the single zircon reflecting transport and entrainment of crystals from greater crustal depths in the magmatic system during magma emplacement, a process well documented in complex plutonic systems (e.g. Samperton et al., 2015). The intermediate analysis is likely from an antecrystic zircon whilst the youngest zircon represents a maximum age of final pluton crystallisation at 32.38 ± 0.03 Ma.

A total of four analyses were made of RT14_024, all the analyses lie off Concordia with excess ^{207}Pb . Two highly discordant dates are significantly older at 97.99 ± 0.09 and 48.45 ± 0.06 Ma, thus are interpreted to be xenocrystic zircons inherited from a much earlier phase of crystallisation in the magmatic system. The youngest analysis is likely an autocrystic zircon and can thus be interpreted as a maximum age of final crystallisation at 32.06 ± 0.07 Ma.

Analyses of RT14_028 range between 32.00 and 32.21 Ma ($^{206}\text{Pb}/^{238}\text{U}$ dates, $n = 5$). One interpretation of these analyses would be that the data represent a single population of zircons with an interpreted $^{206}\text{Pb}/^{238}\text{U}$ geological age of 32.069 ± 0.054 (MSWD = 5.4, $n = 5$), however the MSWD indicates over-dispersion of the data, i.e. they do not represent a statistically significant population (if $n = 5$, MSWD < 2.63 at 2σ confidence levels). We interpret a youngest population of zircons as representative of pluton emplacement with a geological age of 32.045 ± 0.020 Ma (MSWD = 1.15, $n = 3$).

2.2.2 – The Maronia Plutonic Complex

Four samples of the Maronia monzonite were dated and show a strong clustering of antecrystic zircon ages ranging from 29.52 to 29.84 Ma ($^{206}\text{Pb}/^{238}\text{U}$ dates, $n = 17$).

Analyses of RT14_003 range between 29.69 and 29.56 Ma ($^{206}\text{Pb}/^{238}\text{U}$ dates, $n = 3$). An interpretation of these analyses would be that the data represent a single population of zircons with an interpreted $^{206}\text{Pb}/^{238}\text{U}$ geological age of 29.619 ± 0.093 (MSWD = 5.8, $n = 3$), however the MSWD indicates over-dispersion of the data (if $n = 3$, MSWD < 3.83 at 2σ confidence levels). Our favoured approach is to reject the oldest analysis as antecrystic and interpret the youngest two analyses as representative of pluton emplacement with a geological age of 29.619 ± 0.093 Ma (MSWD = 0.79, $n = 2$).

Analyses of MA15_010 range between 29.52 and 29.74 Ma ($^{206}\text{Pb}/^{238}\text{U}$ dates, $n = 5$). Our interpretation of these analyses is that the data represent a single population of zircons with an interpreted $^{206}\text{Pb}/^{238}\text{U}$ geological age of 29.666 ± 0.044 Ma (MSWD = 2.9, $n = 5$); however the MSWD is slightly high indicating mild over-dispersion of the data (if $n = 5$, MSWD < 2.63 at 2σ confidence levels). An alternative approach would be to reject the two oldest analyses as antecrystic and interpret the remaining three analyses as representative of pluton emplacement with a geological age of 29.617 ± 0.035 Ma (MSWD = 0.044, $n = 3$). Both of these interpretations overlap within uncertainty and reflect the robustness of age assignment to variable selection of data for age calculation. Our preferred age is based upon the youngest three $^{206}\text{Pb}/^{238}\text{U}$ dates.

Analyses of MN16_008 range between 29.66 and 29.80 Ma ($^{206}\text{Pb}/^{238}\text{U}$ dates, $n = 5$). Our interpretation of these analyses is that the data represent a single population of zircons with an interpreted $^{206}\text{Pb}/^{238}\text{U}$ geological age of 29.743 ± 0.030 Ma (MSWD = 2.0, $n = 5$). An alternative approach is to select the younger analyses as a zircon crystal population representing of final pluton crystallisation with a geological age of 29.720 ± 0.024 Ma (MSWD = 0.64, $n = 3$).

Analyses of MN16_005 range between 29.71 and 29.84 Ma ($^{206}\text{Pb}/^{238}\text{U}$ dates, $n = 4$) and are concordant within error. These analyses can be interpreted as a single population cluster with a geological age of 29.762 ± 0.017 Ma (MSWD = 0.84, $n = 4$).

2 2.3 Preferred Interpretations

Table 2: Our preferred interpretations of the geological age. Uncertainties: x – analytical uncertainty in the measurements for comparison with other U-Pb data measured within the EARTHTIME framework; y – total uncertainty for comparison of the ages with ages from other isotope systems

<i>Sample ID</i>	<i>Geological Age (Ma)</i>	<i>Uncertainty: x, y</i>	<i>Preferred Interpretation</i>
RT14_010	32.932	± 0.034 ± 0.039	Weighted mean of single population
RT14_009	32.235	± 0.026 ± 0.031	Youngest population of zircons (n = 6, N = 7)
RT14_024	32.06	± 0.07 ± 0.07	Youngest single zircon age
RT14_022	32.38	± 0.03 ± 0.03	Youngest single zircon age
RT14_028	32.045	± 0.020 ± 0.027	Youngest population of zircons (n = 3, N = 5)
MN16_008	29.720	± 0.024 ± 0.034	Weighted mean of single population
MN16_005	29.762	± 0.017 ± 0.024	Weighted mean of single population
RT14_003	29.596	± 0.022 ± 0.027	Youngest population of zircons (n = 2, N = 3)
MA15_010	29.616	± 0.035 ± 0.047	Weighted mean of single population

APPENDIX 3 – Comparison between Rb-Sr and U-Pb Ages

Comparing Rb-Sr and U-Pb ages introduces two additional levels of uncertainty than when comparing ages in the same isotopic system: 1) the uncertainty in our analytical understanding of each system (e.g. the decay constant) and, 2) the uncertainty in the geological interpretation of the ages. The first is an uncertainty associated with turning the measured isotope ratios in a date and can be accounted for in the uncertainty reported with an age. In table 2, the U-Pb zircon ages are reported with two levels of uncertainty where x – analytical uncertainty in the measurement and can be used for comparison within this dataset and other U-Pb data measured within the EARTHTIME (Condon et al., 2015; McLean et al., 2015); and y – total uncertainty in the measurement including the EARTHTIME tracer uncertainty and the decay constant uncertainty and can be compared with other decay systems e.g. Rb-Sr biotite geochronology.

The uncertainty in the geological interpretation of ages between isotopic systems is more difficult to quantify. The U-Pb isotope system has a closure temperature of ~ 900 °C which is greater than the zircon saturation temperature of most intermediate to felsic magma systems (800 – 750 °C), consequently, the U-Pb isotope system in zircon is widely interpreted as closed from crystallization and thus dates zircon crystallization. In most magmatic systems, an additional interpretation that the youngest autocrystic age of a sample represents final crystallization of the pluton is made. In contrast, the closure temperature of the Rb-Sr isotope system in biotite is more difficult to constrain and is quoted between 300 – 400 °C depending on the cooling rate (e.g. Jenkin et al., 2001). This means that a Rb-Sr age dates the timing of magmatic cooling rather than magmatic crystallization. Consequently, the U-Pb and Rb-Sr isotope systems are dating two different geological events which makes Rb-Sr and U-Pb ages incomparable beyond the logical conclusion that the cooling (Rb-Sr) age of a system should be younger than the crystallization (U-Pb) age of that same system. The Rb-Sr biotite ages presented by Del Moro et al., (1988) are remarkably close to the U-Pb zircon ages presented in this study despite much greater uncertainty in the age including the uncertainty in geological interpretation which is not accounted for in the published errors.

References Cited

- Condon, D. J. *et al.* (2015) 'Metrology and traceability of U--Pb isotope dilution geochronology (EARTHTIME Tracer Calibration Part I)', *Geochimica et Cosmochimica Acta*. Elsevier, 164, pp. 464–480.
- Crowley, J. L., Schoene, B. and Bowring, S. A. (2007) 'U-Pb dating of zircon in the Bishop Tuff at the millennial scale', *Geology*, 35(12), pp. 1123–1126. doi: 10.1130/G24017A.1.
- Gerstenberger, H. and Haase, G. (1997) 'A highly effective emitter substance for mass spectrometric Pb isotope ratio determinations', *Chemical geology*. Elsevier, 136(3–4), pp. 309–312.
- Hiess, J. *et al.* (2012) '238U/235U systematics in terrestrial uranium-bearing minerals', *Science*. American Association for the Advancement of Science, 335(6076), pp. 1610–1614.
- Jenkin, G. R. T. *et al.* (2001) 'An investigation of closure temperature of the biotite Rb-Sr system: The importance of cation exchange', *Geochimica et Cosmochimica Acta*. Elsevier, 65(7), pp. 1141–1160.
- Mattinson, J. M. (2005) 'Zircon U--Pb chemical abrasion ("CA-TIMS") method: combined annealing and multi-step partial dissolution analysis for improved precision and accuracy of zircon ages', *Chemical Geology*. Elsevier, 220(1), pp. 47–66.
- McLean, N. M. *et al.* (2015) 'Evaluating uncertainties in the calibration of isotopic reference materials

and multi-element isotopic tracers (EARTHTIME Tracer Calibration Part II)', *Geochimica et Cosmochimica Acta*. Elsevier, 164, pp. 481–501.

Parrish, R. R. (1990) 'U-Pb dating of monazite and its application to geological problems', *Can. J. Earth Sci*, 27(Overstreet 1967), pp. 1431–1450. doi: 10.1139/e90-152.

von Quadt, A. *et al.* (2011) 'Zircon crystallization and the lifetimes of ore-forming magmatic-hydrothermal systems', *Geology*, 39(8), pp. 731–734. doi: 10.1130/G31966.1.

Samperton, K. M. *et al.* (2015) 'Magma emplacement, differentiation and cooling in the middle crust: Integrated zircon geochronological-geochemical constraints from the Bergell Intrusion, Central Alps', *Chemical Geology*. Elsevier B.V., 417, pp. 322–340. doi: 10.1016/j.chemgeo.2015.10.024.

Schärer, U. (1984) 'The effect of initial ^{230}Th disequilibrium on young UPb ages: the Makalu case, Himalaya', *Earth and Planetary Science Letters*, 67(2), pp. 191–204. doi: 10.1016/0012-821X(84)90114-6.

Schmitt, A. K. (2007) 'Ion microprobe analysis of $(^{231}\text{Pa})/(^{235}\text{U})$ and an appraisal of protactinium partitioning in igneous zircon', *American Mineralogist*, 92(4), pp. 691–694. doi: 10.2138/am.2007.2449.

Wendt, I. and Carl, C. (1991) 'The statistical distribution of the mean squared weighted deviation', *Chemical Geology: Isotope Geoscience Section*, 86(4), pp. 275–285. doi: 10.1016/0168-9622(91)90010-T.